DYNAMIC SHOCKS IN THE INHOMOGENEOUS ENVIRONMENT OF THE CYGNUS LOOP

N. A. Levenson,[1] J. R. Graham,[2] and J. L. Walters[2]

RESUMEN

El medio interestelar no homogéneo determina la evolución y apariencia del remanente de supernova del *Rizo del Cisne*. Específicamente, las interacciones de la onda de choque con las nubes interestelares grandes producen casi toda la emisión a frecuencias rayos-X y ópticas de este remanente. Observaciones hechas con el *Chandra X-ray Observatory* y el *Hubble Space Telescope* revelan la onda de choque dinámica y la estructura detallada de las nubes individuales. En algunos casos, notablemente en la orilla occidental, un modelo unidimensional sencillo de la interacción es suficiente, mientras que en otras regiones se requiere discriminar entre proyecciones múltiples o modelos más complejos. A final de cuentas, el *Rizo del Cisne* funge como una sonda muy útil del medio interestelar y como uno de los laboratorios existentes mejores de la física de choques.

ABSTRACT

The inhomogeneous interstellar medium determines the evolution and appearance of the Cygnus Loop supernova remnant. Specifically, interactions of the shock front with large interstellar clouds produce nearly all of this remnant's emission at X-ray and optical wavelengths. Observations with the *Chandra X-ray Observatory* and the *Hubble Space Telescope* reveal the dynamic blast wave and the detailed structure of individual clouds. In some cases, notably the western limb, a simple one-dimensional model of the interaction is sufficient, whereas other regions require discrimination of multiple projections or more complex models. The Cygnus Loop ultimately serves as a useful probe of the interstellar medium and as one of the best existing laboratories of shock physics.

Key Words: **ISM: INDIVIDUAL (CYGNUS LOOP) — SHOCK WAVES — SUPERNOVA REMNANTS — X-RAYS: ISM**

1. INTRODUCTION

Supernova remnants fundamentally drive the cycle of matter and energy in the interstellar medium. Supernova remnants (SNRs) mix newly formed elements into the interstellar medium (ISM), and they may determine whether those elements remain gaseous or enter the solid phase in the form of dust grains. SNRs drive mass exchange between the different phases of the ISM. Each SNR individually consists of an expanding hot interior, which can evaporate surrounding cold clouds. The compression of the ambient medium behind the SNR blast waves sets the stage for future generations of star formation. The interaction between the ISM and the stars in it is reciprocal. The stellar progenitor is responsible for processing the local medium, which alters subsequent evolution of the shock front, while the immediate environment profoundly influences the evolution of an individual SNR.

The bright Cygnus Loop supernova remnant serves as an ideal probe of its surroundings. It is middle-aged ($\tau = 8000$ yr), with the extant ISM determining its subsequent evolution. Because the Cygnus Loop is nearby (440 pc; Blair et al. 1999), it affords high spatial resolution observations with which to investigate the evolution of the blast wave in detail.

As a whole, the Cygnus Loop presents two great problems. First, although the SNR boundary is extremely circular, consistent with a spherical blast wave, it exhibits significant structure and morphological complexity on smaller, though large (10 pc) scales. Second, these outstanding regions tend to exhibit both bright optical emission, characteristic of temperature $T \approx 10^4$ K, and bright X-ray emission, characteristic of $T \approx 10^6$ K. The evolution of the progenitor star and the remaining inhomogeneous ISM account for these observational challenges.

Large clouds and a smooth atomic shell together define the boundary of the cavity the SNR's progenitor created (Levenson et al. 1998), and shocks associated with both clouds and the shell produce X-rays and optical emission. The brightest regions of the Cygnus Loop in optical and X-ray emission are sites of interactions between the SNR blast wave and large interstellar clouds. The blast wave is deceler-

---

[1]University of Kentucky, USA.
[2]University of California, Berkeley, USA.

ated in the dense clouds. The shocks that advance in the clouds are radiative, and their cooling gas emits strongly in many optical lines, including hydrogen Balmer lines, [O III], and [S II], with typical temperature $T \approx 10^4$ K. Shocks that are reflected off the cloud surfaces propagate back through previously shocked material, further heating and compressing it. These reflected-shock regions exhibit enhanced X-ray emission (Hester & Cox 1986) in hot gas.

The primary blast wave also appears in characteristic faint filaments in which Hα and Hβ are the only strong lines in the optical spectrum. Raymond et al. (1980) first identified these in the Cygnus Loop. These "non-radiative" or "Balmer-dominated" shocks excite Balmer line emission through electron collisions in pre-shock gas that is predominantly neutral (Chevalier & Raymond 1978; Chevalier, Raymond, & Kirshner 1980), marking regions where the gas is being shocked for the first time. The excitation is confined to a narrow zone immediately behind the shock front, so these filaments delineate the outer edge of the blast wave. This true boundary of the SNR is now located in the neutral shell of material at the edge of the cavity the progenitor star created.

Here we analyze high spatial resolution, high signal-to-noise observations with the *Chandra X-ray Observatory* (*Chandra*) of two regions of the Cygnus Loop. Both the western limb and southeast knot are sites of interactions between the blast wave and large interstellar clouds, and both also have Balmer filaments that mark the SNR shock front. We view the western limb interaction nearly edge-on, so in this geometrically simple case, one-dimensional modeling is appropriate. The southeast knot is geometrically more complex, offering multiple projections along the line of sight, although the physical conditions are similar. Furthermore, optical images from the *Hubble Space Telescope* (*HST*) reveal this cloud's structure on extremely small scales.

2. THE WESTERN LIMB

The western limb is the archetype of cloud–blast-wave encounters in the Cygnus Loop. The large obstacle is detected directly in molecular observations (Scoville et al. 1997). More importantly, with the edge-on view of the collision, stratification of distinct physical regions is clear, and the simplification to a one-dimensional hydrodynamical problem on small resolved angular scales is reasonable. When the blast wave encounters the cloud, three characteristic regions become important: the decelerated forward shock in the cloud, a reflected shock, and the
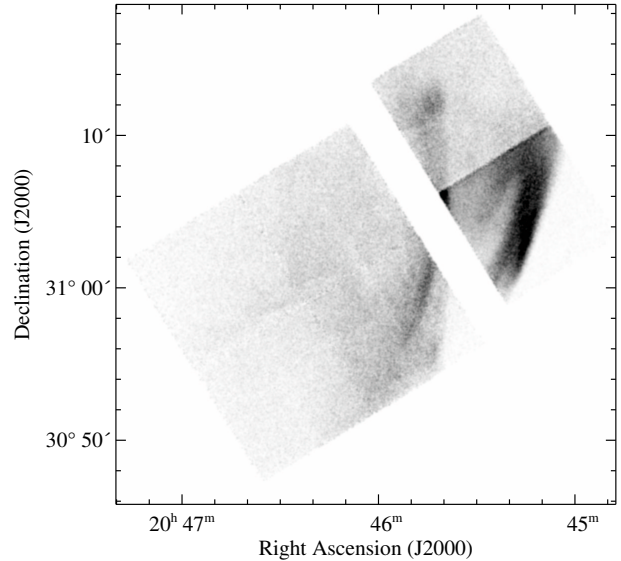

Fig. 1. The western limb of the Cygnus Loop in soft (0.3 to 0.6 keV) X-rays, observed with *Chandra*. The image has been binned by a factor of two and smoothed by FWHM = 14″. It is scaled linearly from 0 (white) to 3×10^{-7} photons cm^{-2} arcsec^{-2} (black).

singly-shocked SNR interior. Because we view the plane of the shock nearly edge-on, the stratification of the spatially distinct emission regions is preserved. The X-ray data we present here also reveal the similar interaction of the primary blast wave with the cavity shell, allowing comparison of these effects in different interstellar conditions.

2.1. *New X-ray Observations*

We obtained a 31 ks exposure of the western limb of the Cygnus Loop on 2000 March 13 and 14 with the *Chandra* Advanced CCD Imaging Spectrometer (ACIS). This instrument allows simultaneous spatial resolution around 1″ and spectral resolution $E/\Delta E \approx 12$ within the $25' \times 17'$ total field of view. (For complete details of the observations and data reduction, see Levenson, Graham, & Walters 2002.)

Comparison of images in several broad energy bands indicate spectral variations, and several of these distinct physical features are evident in the very soft (0.3 to 0.6 keV) X-ray image of Figure 1. (Note that the image is displayed on a uniform linear scale. The westernmost of the six CCDs, centered on right ascension $\alpha = 20^{\mathrm{h}}45^{\mathrm{m}}15^{\mathrm{s}}$, declination $\delta = 31°20'$, is more sensitive to soft X-rays, so the measured count rate is higher, although the flux is not significantly different from that of adjacent regions.)

The hot, diffuse interior of the SNR fills almost all of the observed region. Only the extreme western-

most area ($\alpha < 20^\text{h}45^\text{m}$), which the blast wave has not yet reached, lacks X-rays. The interaction of the blast wave with the large cloud and atomic shell enhances the X-ray emission in most regions within this field ($\alpha > 20^\text{h}46^\text{m}30^\text{s}$). The sharp feature that runs nearly north-south around $\alpha = 20^\text{h}45^\text{m}50^\text{s}$, $\delta = 31°$ is the shock front that propagates through the cloud. Here the shock is still sufficiently fast to produce X-rays, and because the X-ray flux is proportional to n^2, where n is density, the X-rays are bright in this high-density region. The more extended X-ray enhancement toward the east of the cloud shock is due to the additional heating and compression of the reflected shock that propagates back through the previously shocked SNR interior. At the far west of the field, the interaction of the blast wave and the atomic shell similarly enhances X-rays.

To quantify the physical conditions of these distinct features, we extracted spectra from small (roughly $1' \times 15''$) regions. This procedure isolates the regions' particular spectral characteristics and avoids calibration variations that are significant over larger areas. We fit the spectra satisfactorily with thermal equilibrium plasma models, allowing temperature and foreground absorbing column density to be free parameters. We find $kT = 0.03$ and $0.18\,\text{keV}$ in the cloud and reflected shock regions, respectively, at the center of the *Chandra* field. The velocity of the cloud shock is $150\,\text{km\,s}^{-1}$. In the shell and reflected shock regions at the far west, $kT = 0.12$ and $0.16\,\text{keV}$, respectively. The current shock velocity in the shell is $310\,\text{km\,s}^{-1}$, and the original blast wave velocity, prior to this interaction, was $340\,\text{km\,s}^{-1}$.

The intense X-ray emission of the large cloud interaction was previously evident at the spatial resolution of *ROSAT* High Resolution Imager (HRI), but without simultaneous spectral information the decelerated cloud shock and the harder reflected shock could not be distinguished. In these *Chandra* data, however, we uniquely identify both constituents of the X-ray enhancement. The location of the very soft emission further identifies it as the cloud shock. It appears ahead of the harder reflected shock, and it is aligned with the onset of a radiative cooling zone observed optically.

3. THE SOUTHEAST KNOT

Fesen, Kwitter, & Downes (1992) drew attention to the southeast knot, an apparently insignificant feature in the optical and X-ray emission of the Cygnus Loop. The knot is small ($2' \times 4'$) compared with the diameter of the Cygnus Loop ($3°$), and its
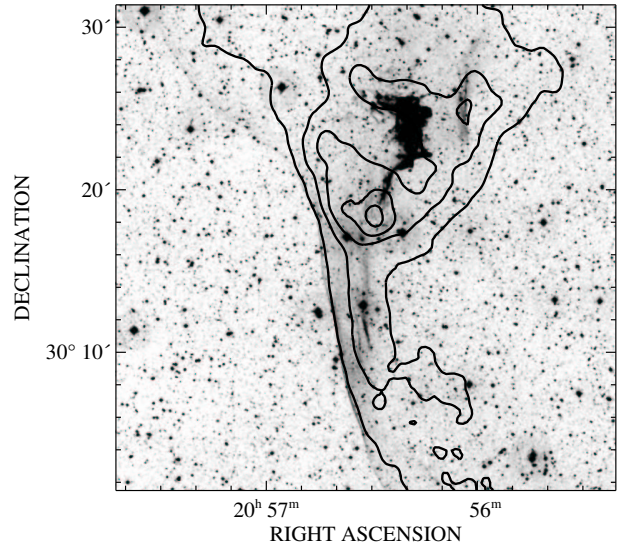

Fig. 2. Hα image of the southeast knot of the Cygnus Loop, scaled logarithmically. Contours of soft X-ray surface brightness measured with the *ROSAT* HRI are overlaid, scaled linearly.

optical appearance suggests that it represents either a minor enhancement in the local ISM, or that the interaction is very young. X-ray imaging supports the latter interpretation. The knot is located at the apex of a large-scale ($0.5°$) indentation in the eastern limb (Graham et al. 1995), so the obstacle must be large, extending at least $5\,\text{pc}$ along the line of sight, and the interaction is therefore at an early stage.

Figure 2 illustrates the relationship between the X-ray and optical emission. Very faint Hα filaments at the east mark the current location of the blast wave. The cloud itself is relatively bright, and another filament appears in projection west of the cloud. Faint soft X-rays follow behind the blast wave, but the brightest X-ray region is located southeast of the optical cloud. Enhanced X-rays are also detected near the western Hα filament.

3.1. *New X-ray Observations*

While entirely covering the region of interest, these *ROSAT* X-ray data do not provide any spectral information. Thus, we observed the southeast knot with *Chandra* in order to determine the physical characteristics over a more limited spatial extent. On 2000 September 1, we obtained a $46\,\text{ks}$ exposure of the southeast knot with ACIS. We processed the data in the same way we had processed the observations of the western limb. The southeastern region shows much less significant variation in both total intensity and spectral character. While similar sim-
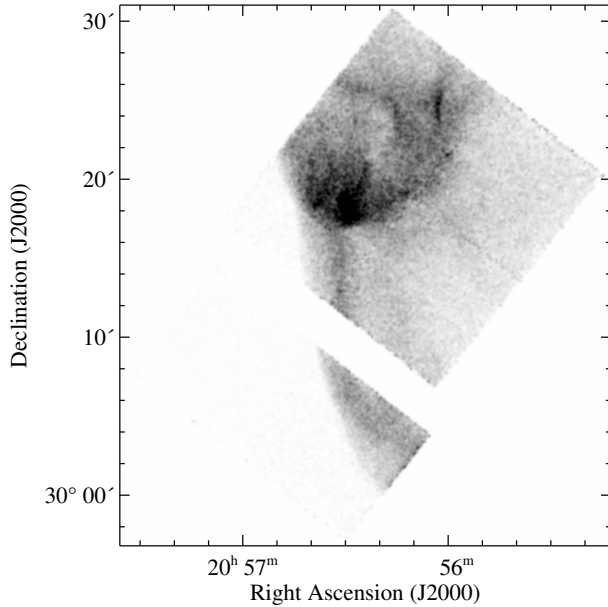
Fig. 3. The southeast knot of the Cygnus Loop in soft (0.3 to 0.6 keV) X-rays, observed with *Chandra*. The image has been binned by a factor of two and smoothed by FWHM $= 14''$. It is scaled linearly from 0 (white) to 3×10^{-7} photons cm^{-2} arcsec^{-2} (black).

ple physical models of collisional shock excitation are still applicable, the geometry of this region is complex.

Figure 3 shows the very soft (0.3 to 0.6 keV) X-ray emission. (In this case, the sensitivity of all the detectors that observed the SNR is similar.) We compare with images in two other energy bands (0.6 to 0.9 and 0.9 to 2 keV) in order to identify small regions for spectroscopy. We combine the spectroscopic and imaging results in order to understand the physical circumstances of this cloud/blast-wave interaction.

We identify several features in the X-ray image in Figure 4. Similar to the western limb, the cloud shock is evident in the soft X-ray image. This shock is not a flat plane, but instead curves around the cloud, tracing its outline. Once again, with spectroscopic information, we find that the forward shock in the cloud produces much of the X-ray enhancement of the cloud interaction; the reflected shock alone does not completely account for the observed X-rays. In the southeast knot, the extended optically bright cloud corresponds to an X-ray faint region. The blast wave in the bulk of the cloud is not fast enough to produce strong X-ray emission, and the cloud itself absorbs much of the soft X-ray emission that would be detected along this line of sight due to any background projection.

Toward the east of this field, we observe several projections of the primary shock front. At the far east, these X-ray enhancements are associated with Balmer-dominated filaments and therefore represent the true projected edge of the blast wave. Similar to the western shell, the corresponding X-ray enhancements are due to the increased density encountered in the atomic shell. They are much too narrow ($40''$) to be the swept-up shell of the interstellar medium of a SNR in the Sedov-Taylor stage, which would be about $7'$ wide. As observed in the *ROSAT* HRI data, the large-scale indentation of the spherical shell is also apparent here. The cloud must extend along the line of sight, obstructing the entire three-dimensional surface of the blast wave. Thus, the cloud is much larger than the optically bright or X-ray-detected cloud shock suggests.

The X-ray-bright spot southeast of the cloud is a consequence of the multiple projections along the same line of sight, where we detect the emission from a larger volume of denser shocked material. This spot is only about twice as bright as the X-ray enhancements associated with the Balmer filaments, and therefore requires only two overlapping shocks. Extensions of the two Balmer filaments (and X-ray enhancements) east and south of the bright spot are probably its origin. As we show below, the spot is not spectrally distinct from other singly shocked regions behind the blast wave.

Another region of enhanced emission toward the northwest of this field is yet another projection of the spherical blast wave. This X-ray feature is also associated with a Balmer-dominated filament offset to the east. Thus, this region is being shocked for the first time. The increased X-ray emission is located toward the interior of the SNR, and this projection of the blast wave also moves toward the east.

We extracted spectra from several small regions of interest, isolating distinct spectral or morphological features in the images. We fit thermal equilibrium plasma models to the spectra. We find $kT = 0.06$ keV in the decelerated shock at the edge of the cloud, which is still fast enough ($v_s = 220$ km s^{-1}) to produce soft X-rays. At the east, we find similar spectra in all regions, including those associated with Balmer filaments and the bright spot. We measure $kT = 0.11$ keV in these locations.

The diffuse, low-surface-brightness emission throughout the remainder of this southeastern field is the hot interior of the SNR. We find $kT = 0.18$ keV in the diffuse interior. This temperature corresponds to $v_s = 380$ km s^{-1} in the undisturbed blast wave, which is slightly higher than the values determined
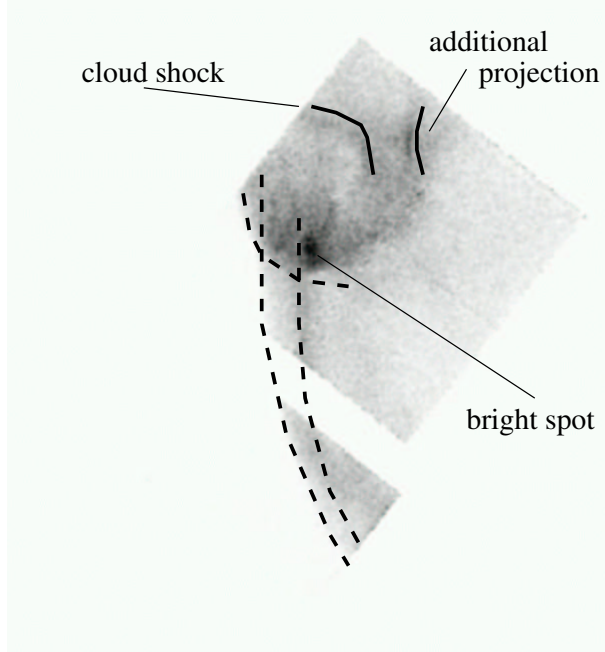
Fig. 4. The soft X-ray image of the southeast knot of the Cygnus Loop, with several features identified. Brighter soft X-rays define the cloud shock, and the optically bright slower shocks in the cloud correspond to an X-ray-faint region south and east of the cloud shock. Several projections of the exterior blast wave are marked with dashed lines.

from the observations of the western limb. The measured temperatures of the singly shocked SNR interior and the cloud shock correspond to a density contrast of 7 between the cloud and the ambient cavity interior. Assuming the cloud has a gradual density gradient toward its interior, rather than a sharp edge, this value underestimates the true contrast with the bulk of the cloud. The strong optical emission that shocks in the cloud interior produce demonstrates that the blast wave is further decelerated as it propagates through the southeast cloud.

In all of the X-ray spectroscopy of both the southeast and western limb observations, we fit the data with equilibrium collisional ionization models. We also considered the effect of non-equilibrium ionization. Ionization is not immediate following the passage of a shock, so the line-producing elements are initially underionized relative to their equilibrium values. Achieving equilibrium is a function of the electron density, n_e, and time elapsed since the shock passage, t. Ionization equilibrium usually occurs when $n_e t \geq 3 \times 10^{11} \, \mathrm{cm}^{-3} \, \mathrm{s}$, depending on the element and its equilibrium state. The best-fitting non-equilibrium models we considered tend toward equilibrium solutions, with $n_e t \gg 10^{12} \, \mathrm{cm}^{-3} \, \mathrm{s}$. On
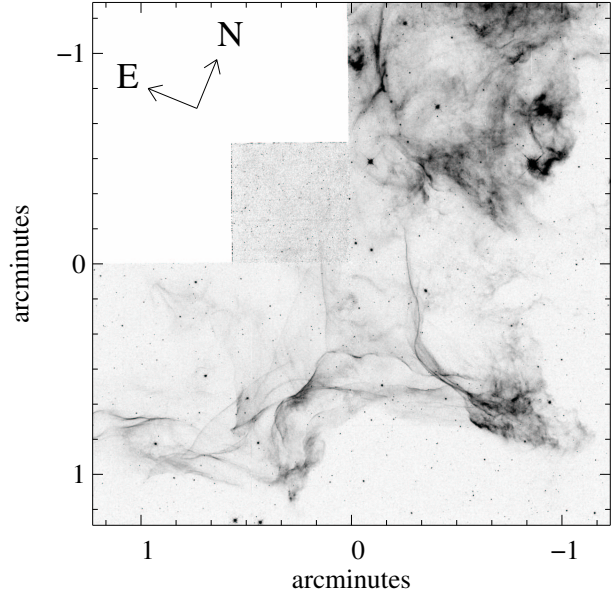

Fig. 5. The Hα emission from the southeast knot of the Cygnus Loop, observed with *HST*. The image is scaled linearly from 0 (white) to $4 \times 10^{-14} \, \mathrm{ergs} \, \mathrm{cm}^{-2} \, \mathrm{s}^{-1} \, \mathrm{pixel}^{-1}$ (black).

physical grounds, we would expect non-equilibrium conditions to be marginally relevant. At the very soft X-ray energies of the Cygnus Loop, however, no instrument has the spectral resolution and sensitivity on small spatial scales required to measure the non-equilibrium conditions directly and accurately. The spectra of a fully equilibrated lower temperature medium and the non-equilibrium state of a higher temperature plasma remain indistinguishable, so we adopt the better-fitting equilibrium models to interpret these data.

3.2. *High-Resolution Optical Imaging*

Smaller-scale variations are present, which high-resolution optical images reveal. *HST* observed the southeast knot with the Wide-Field Planetary Camera 2 on 1994 November 25 (PI J. Hester) through three filters that include prominent emission from Hα, [O III], and [S II] lines. (See Levenson & Graham 2001 for complete details of the data reduction and analysis.) We detect variations on the smallest resolvable scales (7×10^{14} cm), which we attribute to pre-existing inhomogeneities in the cloud surface.

The Hα image of the southeast knot (Figure 5) illustrates two characteristic morphologies: sharp filaments and diffuse emission. These two morphologies are also evident on larger scales within the Cygnus Loop. The two types of emission correspond to two distinct viewing geometries of the thin sheet of

shocked material (Hester 1987). Sharp filaments are detected when the sheet is viewed edge-on, through tangencies. In general, these shocks propagate in the plane of the sky. This is the most favorable geometry for viewing the stratification of the postshock flow as it cools and recombines. Comparison with the other images reveal in turn the Balmer- and [O III]-dominated regions behind the shock front. In contrast, diffuse emission corresponds to face-on views of the shock front, propagating along the line of sight. Because larger swept-up column densities are required for this diffuse emission to be detectable, it is more likely to exhibit the characteristics of a complete radiative shock, namely strong [S II] relative to [O III] and Hα.

The relationship between Balmer filaments and downstream [O III] emission of incomplete shocks distinguishes the physical conditions that are present. The key parameter that determines the location and width of the [O III] emission zone is swept-up column density behind the shock front, so the [O III] surface brightness profile constrains the ambient density and shock velocity. In general, [O III] emission rises gradually and closer to slower shock fronts, while the profile is sharply peaked and offset farther downstream from fast shocks. We compare these *HST* observations with updated models of Raymond (1979) and Cox & Raymond (1985), finding $v_s = 170\,\mathrm{km\,s^{-1}}$ and $n = 15\,\mathrm{cm^{-3}}$ in one particularly clear example at the center of the field.

The pressure driving this shock in the southeast cloud is much greater than the pressure of the primary blast wave. Using the parameters above, $\rho v^2 = 7 \times 10^{-9}\,\mathrm{dyne\,cm^{-2}}$ is an order of magnitude greater than the blast-wave pressure derived from global X-ray data (Ku et al. 1984), $P_{\mathrm{BW}} = 5 \times 10^{-10}\,\mathrm{dyne\,cm^{-2}}$. Some overpressure is expected in all cases where the blast wave encounters a density enhancement. The effect is greater when the blast wave encounters a plane of material compared with the case in which steady flow is reestablished following an encounter with a small cloud. Thus, the very large overpressure measured in the southeast knot supports the interpretation of this case as the very early stage of interaction between the blast wave and a large interstellar cloud.

4. CONCLUSIONS

The western limb and the southeast knot of the Cygnus Loop offer two examples of the interaction of the SNR blast wave with large interstellar clouds. The presence of such large clouds at the perimeter of the progenitor's cavity account for the SNR's circular appearance. These inhomogeneities in the ISM are necessary, however, to produce the strong observed correlation between the optical and X-ray views. Before the shock front reached these high-density regions at the cavity boundary, the SNR was faint at both optical and X-ray wavelengths. Both the western limb and the southeast knot represent very early times of interaction between the blast wave and the clouds. The shock will not ultimately destroy such large clouds. Instead, the presence of so many large clouds around the SNR's perimeter will profoundly reduce the final size of the SNR and its total heating of the ISM compared with evolution in a homogeneous environment.

REFERENCES

Blair, W. P., Sankrit, R., Raymond, J. C., & Long, K. S. 1999, AJ, 118, 942

Chevalier, R. A., & Raymond, J. C. 1978, ApJ, 225, L27

Chevalier, R. A., Raymond, J. C., & Kirshner, R. P. 1980, ApJ, 235, 186

Cox, D. P., & Raymond, J. C. 1985, ApJ, 298, 651

Fesen, R. A., Kwitter, K. B., & Downes, R. A. 1992, AJ, 104, 719

Graham, J. R., Levenson, N. A., Hester, J. J., Raymond, J. C., & Petre, R. 1995, ApJ, 444, 787

Hester, J. J. 1987, ApJ, 314, 187

Hester, J. J., & Cox, D. P. 1986, ApJ, 300, 675

Ku, W. H.-M., Kahn, S. M., Pisarski, R., & Long, K. S. 1984, ApJ, 278, 615

Levenson, N. A., Graham, J. R., Keller, L. D., & Richter, M. J. 1998, ApJS, 118, 541

Levenson, N. A., & Graham, J. R. 2001, ApJ, 559, 948

Levenson, N. A., Graham, J. R., & Walters, J. L. 2002, ApJ, 576, 798

Raymond, J. C. 1979, ApJS, 39, 1

Raymond, J. C., Davis, M., Gull, T. R., & Parker, R. A. R. 1980, ApJ, 238, L21

Scoville, N. Z., Irvine, W. M., Wannier, P. G., & Predmore, C. R. 1977, ApJ, 216, 320

James R. Graham and Julie L. Walters: Department of Astronomy, University of California, Berkeley, CA 94720, USA (jrg, jwalters@astro.berkeley.edu).

Nancy A. Levenson: Department of Physics and Astronomy, University of Kentucky, Lexington, KY 40506, USA (levenson@pa.uky.edu).